Dalton Transactions

PAPER

View Article Online
View Journal | View Issue

Cite this: *Dalton Trans.*, 2016, **45**, 9174

Incorporation of gallium-68 into the crystal structure of Prussian blue to form $K^{68}Ga_xFe_{1-x}[Fe(CN)_6]$ nanoparticles: toward a novel bimodal PET/MRI imaging agent†

Murthi S. Kandanapitiye,[a] Matthew D. Gott,[b] Andrew Sharits,[c] Silvia S. Jurisson,[b] Patrick M. Woodward[c] and Songping D. Huang*[a]

Received 14th March 2016,
Accepted 5th May 2016

DOI: 10.1039/c6dt00962j

www.rsc.org/dalton

Similarity between the Ga^{+} ion and the Fe^{3+} ion allows for partial replacement of Fe^{3+} ions with Ga^{3+} ions in the Fe(III) crystallographic positions in Prussian blue (PB) to form various solid solutions $KGa_xFe_{1-x}[Fe(CN)_6]$ ($0 < x < 1$). Such solid solutions possess very high thermodynamic stability as expected from the parent PB structure. Consequently, a simple one-step ^{68}Ga-labeling method was developed for preparing a single-phase nanoparticulate bimodal PET/MRI imaging agent based on the PB structural platform. Unlike the typical ^{68}Ga-labelling reaction based on metal complexation, this novel chelator-free ^{68}Ga-labeling reaction was shown to be kinetically fast under the acidic conditions. The Ga^{3+} ion does not hydrolyze, and affords the ^{68}Ga-labelled PB nanoparticles, which are easy to purify and have extremely high stability against radionuclidic leaching in aqueous solution.

Introduction

Diagnostic nuclear medicine consists of two major imaging modalities, namely, single photon emission computed tomography (SPECT) and positron emission tomography (PET).[1,2] SPECT uses radiotracers labelled with a γ-emitting radionuclide, which is measured directly using a γ-camera to generate 3D images using tomographic reconstruction algorithms. On the other hand, PET relies on the detection of the two photons emitted on electron-positron annihilation. After data acquisition, similar computer-based tomographic reconstruction algorithms are used to generate 3D images. Among the currently used γ-emitting radionuclides suitable for SPECT, such as ^{123}I, ^{111}In, ^{67}Ga, ^{99m}Tc, and ^{201}Tl, ^{99m}Tc continues to be the isotope of choice for diagnostic nuclear medicine owing to its near ideal nuclear properties, versatile coordination chemistry, and availability from a $^{99}Mo/^{99m}Tc$ generator.[3–6] However, the recent global supply shortage of this radionuclide due to the aging nuclear reactors in Europe and North America has highlighted potential issues in the availability of this radionuclide.[7–9] There is an interest in alternative radionuclides, and especially positron-emitters in part due to the improved resolution with PET and the ability to quantitate. This has led to an increased focus on the medicinal and radiopharmaceutical chemistry of gallium relevant to radiolabelling ^{68}Ga.[7,8,10–13] As a positron emitter (1.899 MeV, 89%), ^{68}Ga has a half-life of 68 minutes, which is long enough to allow preparation and purification of ^{68}Ga-labeled radiopharmaceuticals and for PET imaging, but not for long-range shipping of the radioisotope or the ^{68}Ga-labeled radiopharmaceuticals. The advent of the $^{68}Ge/^{68}Ga$ generator system has eliminated the need for an onsite cyclotron.[10] This development is responsible for the widespread use of ^{68}Ga-labeled radiopharmaceuticals at hospitals and clinical centres in many countries around the globe. In contrast to technetium, however, the coordination chemistry of gallium is limited to that of oxidation state +3 under physiologically relevant conditions.[7,13,14–16] At pH > 3, the Ga^{3+} ion hydrolyzes to form insoluble $Ga(OH)_3$, which would redissolve at pH > 7, to form the $[Ga(OH)_4]^-$ ion. Both features can complicate or even hinder radiolabeling reactions. Furthermore, the Ga^{3+} ion closely resembles the Fe^{3+} ion in several important aspects including ionic charge, ionic radius (Ga^{3+} = 0.62 Å *vs.* Fe^{3+} = 0.65 Å for the high-spin electron configuration), electron configuration, and coordination number (*i.e.*, typically CN = 6). In general, the formation constants of the typical Ga^{3+} complexes are consistently lower than those of

[a]*Department of Chemistry and Biochemistry, Kent State University, Kent, OH 44240, USA. E-mail: shuang1@kent.edu*
[b]*Department of Chemistry, University of Missouri, Columbia, MO 65211, USA*
[c]*Department of Chemistry and Biochemistry, The Ohio State University, Columbus, Ohio 43210, USA*

†Electronic supplementary information (ESI) available. See DOI: 10.1039/c6dt00962j

the Fe^{3+} counterparts. Due to the lack of the Ligand Field Stabilization Energy (LFSE), the high-spin Fe^{3+} complexes may be thermodynamically stable, but kinetically labile. This is the reason that most current ^{68}Ga-labelling studies for *in vivo* applications involve the multidentate macrocyclic ligands including HBED, THP, DOTA, NOTA and the other analogues to ensure high thermodynamic stability. Similarly, most Ga^{3+}-complexes have been shown to be kinetically labile and susceptible to *in vivo* decomplexation, transmetallation and hydrolysis when delivered as a complex. Currently, the continuing interest in the coordination and bioconjugate chemistry of gallium is largely focused on addressing these issues.[17–20]

On the other hand, use of nanoparticulate platforms in different imaging modalities represents a paradigm shift in the development of cellular imaging probes.[21–25] Nanoparticle-based imaging agents, particularly those with particle size smaller than 10 nm and coated with a highly water-soluble polymer, can have a greater blood circulation half-life than the molecular counterparts, and may also be preferred platforms for developing multiple imaging modalities. In addition, nanoparticles with proper sizes and surface characteristics may exhibit phagocytic internalization into cells and can be surface-modified with a targeting agent for targeted cellular and molecular imaging applications. However, incorporation of ^{68}Ga into nanoparticles for PET or multiple modal imaging is currently a neglected field of research. Recently, Archibald and co-workers investigated ^{68}Ga-labelling of iron oxide nanorods coated with various mixtures of PEG and a macrocyclic ligand tetraazamacrocyclic chelator (DO3A) *via* the formation of a silica layer on the surface and demonstrated that the nanoconstructs possess high stability in human serum.[26] Furthermore, they showed that in the presence of the silica coating, the DO3A ligand was not even required for preparation of highly stable radiometal-NP constructs for *in vivo* PET-CT and MR imaging applications.[27] Previously, we demonstrated that Prussian blue nanoparticles (PBNPs) have the ability to function as a T_1-weighted MRI contrast agent due to the superparamagnetic nature of PB (T_B = 4.5 K).[28,29] We showed that PBNPs have no cytotoxicity and can be readily internalized by cells to act as effective cellular MRI probes.[29] Interestingly, gallium forms an analogue of soluble PB (SPB) with the formula $KGa[Fe(CN)_6]\cdot 4H_2O$ that crystallizes in the same faced-cantered structure as the parent PB does (space group $Fm\bar{3}m$). The NPs of $KGa[Fe(CN)_6]\cdot 4H_2O$ exhibit no cytotoxicity and can be internalized by cells, albeit they are diamagnetic, and do not function as an MRI contrast agent.[30] In this publication, we describe the synthesis and characterization of both bulk and nanoparticulate forms of $KGa_xFe_{1-x}[Fe(CN)_6]$ ($0 \le x \le 1$) solid solutions. We found that such solid solutions possess superb thermodynamic stability and kinetic inertness. The latter will prove to be more important at high dilution under *in vivo* conditions where equilibrium conditions do not exist. We also found that these solid NPs solutions have no cytotoxicity and can be internalized by cells, and thus are a suitable platform for developing single-compound-based bimodal PET/MRI imaging agents.

Results and discussion

Our approach to synthesizing nanoparticles of nonradioactive Ga-incorporated Prussian blue solid solutions exploited a simple aqueous solution-based procedure previously developed for the synthesis of $KGa[Fe(CN)_6]$ NPs.[30] To test the adaptability of this synthetic method for preparing Ga(III)–Fe(III) PB solid solutions, a bulk sample of $KGa_{0.05}Fe_{0.95}[Fe(CN)_6]$ was prepared by reacting an aqueous solution containing 0.9 mM $Fe(NO_3)_3$ and 0.1 mM $Ga(NO_3)_3$ with an aqueous solution of 1 mM $K_4[Fe(CN)_6]$ at room temperature. Upon mixing the two solutions, a deep-blue colloidal solution immediately formed. Prolonged stirring at room temperature afforded a fine precipitate that was separated by centrifugation, purified by dialysis and collected by lyophilisation. Powder X-ray diffraction (XRD) studies showed that the sample prepared under these conditions possesses moderate crystallinity as demonstrated by the broad peaks, but nevertheless the material is phase pure and can readily be indexed to the expected cubic face-centred PB structure in the space group of $Fm\bar{3}m$. This synthetic procedure was extended to make four large samples of the solid solutions in the series $KGa_xFe_{1-x}[Fe(CN)_6]$ with x = 0.02, 0.05, 0.07 and 0.10 for structural characterization using the powder XRD method. To increase crystallinity of the samples, the preparations were carried out in a Teflon-lined autoclave at 90 °C. However, the hydrolysis of Fe(III) and Ga(III) at this temperature competed with the formation of Ga-incorporated PB solid solutions and resulted in products contaminated with the Fe(III) and Ga(III) oxides. This difficulty was overcome by using a small amount of hydrochloric acid in each reaction, which did not interfere with the incorporation of Ga(III) into the PB structure to form solid solutions. This observation is consistent with the fact that single crystals of PB and several of its transition metal analogues can be grown from the concentrated HCl medium.[31,32] All four crystalline bulk samples were characterized by elemental analysis of Ga and Fe, and Rietveld refinement using powder X-ray data (*vide infra*). The results from the metal analysis revealed a large discrepancy between the nominal composition used in the synthesis and the actual formula derived from the metal ratio of the elemental analysis. Specifically, approximately half of the Ga(III) ions added to the solution were incorporated in the products. In other words, the efficiency of Ga-incorporation is roughly 50%. The exact mechanism of how the Ga-incorporated solid solutions form under these conditions remains unclear. Since crystallinity is not required to evaluate their potential for biomedical applications, the aforementioned solution method was used to synthesize $KGa_{0.05}Fe_{0.95}[Fe(CN)_6]$ nanoparticles (Ga@PBNPs) in order to avoid the hydrolysis side reaction and prevent the aggregation of the nanoparticulate products. In the presence of polyvinylpyrrolidone (PVP) and citric acid as the capping agents, mixing of the two aqueous solutions gave a clear bright blue colloidal dispersion, and no precipitate was formed with prolonged stirring at room temperature.

The TEM studies showed that Ga@PBNPs have cubic or rectangular-prism shape with an average size of 60 ± 10 nm, while

the dynamic light scattering (DLS) measurements gave ~90 nm as the average solution hydrodynamic diameter for such NPs (see Fig. S1 of the ESI†). Furthermore, the NPs exhibited quasi-single crystal features as shown by their TEM images and confirmed by the selected area electron diffraction (SAED) patterns of the randomly selected individual NPs (Fig. 1). Energy dispersive X-ray spectroscopy (EDX) of such PVP-citrate coated Ga@PBNPs showed distinctive signals for K, Ga, Fe, C and N (see Fig. S2 of the ESI†). Elemental mapping of such NPs acquired in the drift-corrected STEM-EDX mode showed uniform distribution of these elements, suggesting that the Ga(III) ions are incorporated into the PB structure to form a single-phased solid solution instead of a mechanical mixture of $KFe[Fe(CN)_6]$ and $KGa[Fe(CN)_6]$ nanoparticles (see Fig. S3 of the ESI†). The XRD patterns of PVP-citrate coated Ga@PBNPs can be unambiguously indexed to the same cubic $Fm\bar{3}m$ structure, albeit the peaks are considerably broader than those from the bulk materials due to the Debye-Scherrer broadening effect (see Fig. S4 of the ESI†). The average particle size estimated from the XRD patterns is considerably smaller (*i.e.*, approximately 10 nm) than the size measured from the TEM images, as this is often the case when nanoparticles possess varying thickness and different shapes.

The PVP-citrate coated Ga@PBNPs obtained have excellent water dispersibility with a concentration as high as 10 mg mL^{-1} of NPs readily dispersible in distilled water. Additionally, the aqueous dispersions of such NPs have excellent stability against aggregation. For over 3 months, the hydrodynamic size of the dispersions stored at room temperature remained unchanged. We attribute these desirable properties to the concomitant use of both PVP and citrate as the capping agents in the synthesis. As a matter of fact, neither PVP nor citrate alone adequately stabilizes Ga@PBNPs. An additional advantage of using citrate as a coating agent is that it forms transiently stable complexes with the trivalent cations Ga(III) and Fe(III). Such complexes gradually release the trivalent cations to react with the $[Fe(CN)_6]^{4-}$ ion. This ligand-displacement reaction acts to control the rate of nucleation in the formation of Ga@PBNPs. This complexation reaction might have also played a role in preventing the formation of the $Fe(OH)_3$ and $Ga(OH)_3$ by-products in parallel with the formation of the desired Ga@PBNPs. The results from thermal gravimetric analysis (TGA) showed that the average surface loading of PVP and citrate was 42.6 wt% (see Fig. S5 of the ESI†). The latter cannot be removed from the surfaces of NPs by repetitive dialysis against deionized water. The Fourier transform infrared (FTIR) spectra of the dialyzed Ga@PBNPs exhibited the characteristic C≡N stretching vibration at 2061 cm^{-1} for the Fe^{2+}–C≡N–M^{3+} (M = Fe and Ga) unit. The same band was also observed in the bulk $KGa_{0.02}Fe_{0.98}[Fe(CN)_6]$ sample. In addition, all the characteristic bands for both PVP and citrate were observed in the Ga@PBNP sample, suggesting that the capping agents are strongly attached to the NP surfaces, and the prolonged dialysis did not result in their removal from the NPs (see Fig. S6 of the ESI†).

The crystal structures of four samples of the solid solutions of $KGa_xFe_{1-x}[Fe(CN)_6]$ (x = 0.02, 0.05, 0.07 and 0.10) were determined by powder X-ray diffraction (XRD) on bulk samples and found to be isostructural with the well-known soluble Prussian blue (SPB) structure reported by Ludi *et al.* using single-crystal structure analysis.[31] The Rietveld refinement was performed using TOPAS academic software (Fig. S7 in the ESI†).[33] Atomic positions of $KNi[Fe(CN)_6]_{0.3}[Co(CN)_6]_{0.7}$ from the work by Widmann and co-workers were used as the starting point of the refinement.[34] The final parameters from the refinement are summarized in Tables S1 and S2 of the ESI.† The structure can be best described as the face-centred cubic structure defined by one type of ion (*i.e.*, the Fe^{2+} or M^{3+} (M = Fe or Ga) ions) with another type of ion (*i.e.*, the M^{3+} or Fe^{2+} ions) occupying the octahedral holes. The infinite 3D framework structure is then completed by the coordination of the CN^- groups (Fig. 2), with half of the tetrahedral sites in the crystal structure occupied by K^+ ions. Substitution of Ga(III) for Fe(III) in the solid solutions showed a steady decrease in the unit cell parameter as reflected in the difference of their ionic radii (*i.e.*, Fe(III) = 69 pm and Ga(III) = 62 pm). Furthermore, the trends of decreasing unit cell parameters in these solid solutions are linear and obey Vegard's Law (see Fig. S8 of the ESI†).

To assess the stability of the bulk solid solution $KGa_{0.05}Fe_{0.95}[Fe(CN)_6]$ against leaching of metal ions in aqueous solution, its solubility product constant was determined by solution conductivity measurements.[35] The equili-

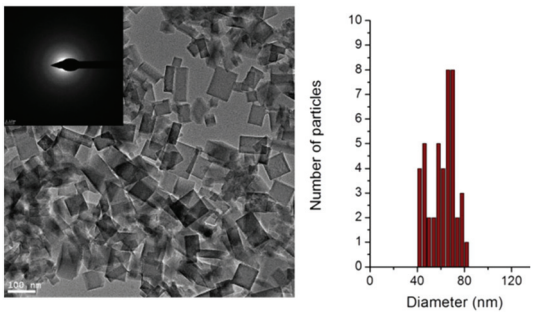

Fig. 1 The TEM image of PVP-citrate coated Ga@PBNPs with a selected-area electron diffraction map (left) and the histogram of particle size distribution (right).

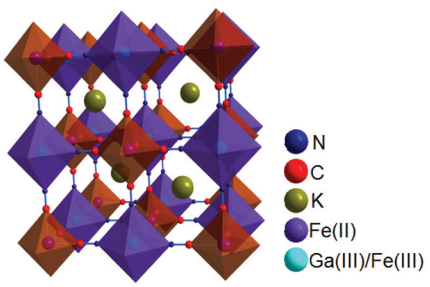

Fig. 2 Polyhedral representation of the $KGa_xFe_{1-x}[Fe(CN)_6]$ (x = 0.02, 0.05, 0.07 and 0.10) structure.

brium concentration for each ion K^+, M^{3+} (M = Fe + Ga) and $[Fe(CN)_6]^{4-}$ was calculated to be 2.8×10^{-10} M from these measurements, which results in a solubility product constant for $Ga_{0.05}Fe_{0.95}[Fe(CN)_6]$ of $2.2 \pm 3 \times 10^{-29}$ mol^3 L^{-9}. In other words, the leachate is most likely to contain the released metal ions at the nanomolar level. To further confirm this assessment, the concentrations of iron and gallium ions released by such bulk samples were measured by atomic absorption spectroscopy (AAS). Since the expected concentrations of the two metal ions were well below the detection limit of this analysis method, the leachate was pre-concentrated before the determination of metal ion concentration by AAS was carried out. The results showed that the leachate contained *ca.* 49 ± 3 nM of iron, but no gallium was detected even after pre-concentration of the leachate. We also conducted leaching experiments with either bulk samples or NPs of $Ga_{0.05}Fe_{0.95}[Fe(CN)_6]$ in a saline solution and blood serum at 37 °C, respectively, using a similar procedure as described in the above. In all such experiments, gallium was not detected in the pre-concentrated leachates. The extremely low leaching level of Ga^{3+} ions offers a rare opportunity for such NPs as a delivery vehicle for the ^{68}Ga isotope. A ^{68}Ga-labelling kit was developed where aqueous $Fe(NO_3)_3$ and $K_4[Fe(CN)_6]$ solutions with the proper coating agents were pre-made and sealed in two separate vials. After ^{68}Ga was eluted from the generator as $^{68}GaCl_3$ in 0.1 M HCl solution, the above three solutions in the appropriate ratio were mixed and shaken for 1 minute to give a blue solution containing ^{68}Ga-labelled PB nanoparticles. The solution was immediately transferred into a dialysis bag and purified by dialyzing against distilled water for 9 minutes (see the Experimental section for details). The entire labelling process took only 10 minutes to complete. The labelling efficiency was estimated to be >99.9%. As shown in Fig. 3, the purified ^{68}Ga-labelled PB nanoparticles were very stable against leaching of radionuclides (*i.e.*, the radioactivity detected in the outside aqueous solution was indistinguishable from the background level of radioactivity even after accounting for the spontaneous decay of ^{68}Ga).

Additionally, the proton T_1 and T_2 relaxation measurements showed that Ga@PBNPs can act as an MRI contrast agent due to the presence of the paramagnetic Fe(III) ion ($S = 5/2$) in these NPs. The r_1 and r_2 values were found to be 0.43 mM^{-1} s^{-1} and 0.77 mM^{-1} s^{-1}, respectively, at a magnetic field of 1.4 Tesla using a Bruker MiniSpec relaxometer (see Fig. S9 of the ESI†). These values are small compared to those of typical T_1-weighted contrast agents currently used in clinical MR imaging (*e.g.*, Magnevist®) with r_1 = 3.4 mM^{-1} s^{-1} and r_2 = 3.7 mM^{-1} s^{-1} at the same magnetic field strength.[36] It should be noted that ^{68}Ga-based PET is a highly sensitive imaging modality, which makes the proton relaxivities in Ga@PBNPs mismatched with the positron-emitting sensitivity of the ^{68}Ga ions incorporated in these NPs.[37] We recently reported that the K^+ ions situated in the tetrahedral holes of the PB structure can be partially substituted by the Gd^{3+} ions to form a solid solution $Gd_xK_{1-3x}Fe[Fe(CN)_6]$ with x = 0.02 (Gd@PBNP).[38] The nanoparticles of the latter solid solution have r_1 = 16.4 mM^{-1} s^{-1} and r_2 = 20.9 mM^{-1} s^{-1}, which readily places Gd@PBNPs among the best NP-based MRI contrast agents.[38] Given the potential presented by this novel approach to increasing proton relaxivities in the PB system, it is possible that incorporation of gadolinium into the current Ga@PBNPs may lead to a new Gd + Ga@PBNPs with proton relaxivities suitable for bimodal PET/MRI imaging applications using the latter NPs. Work is under way to develop such imaging agents.

To explore the potential of developing either a standalone PET or a bimodal PET/MRI imaging agent based on this structural platform, the *in vitro* cytotoxicity of Ga@PBNPs was examined using an MTT assay. HeLa cells were incubated for 24 hours with varying amounts of these NPs. Three independent trials were carried out with the results averaged. Cell viability was then expressed as the percentage viability for each concentration tested in comparison untreated cells as the control with cell viability set as 100%. As shown in Fig. 4, the results clearly demonstrate that Ga@PBNPs are nontoxic to HeLa cells. For instance, at the highest concentration (1.16 mM) of NPs used for this study, the cell viability was found to be 94 ± 4%, indicating that the PVP-citrate coated Ga@PBNPs exhibit minimal cytotoxicity. These findings are consistent with the previous observations that the NPs of the parent compounds KFe$[Fe(CN)_6]$ and KGa$[Fe(CN)_6]$ are nontoxic to cells.[30]

The ability of Ga@PBNPs to cross the cell membrane would offer an important opportunity to develop them as cellular

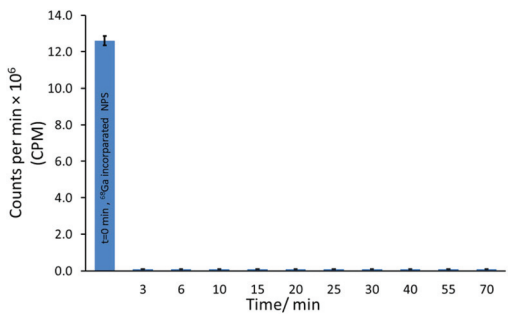

Fig. 3 Time-dependent leaching of the ^{68}Ga radioactivity from the ^{68}Ga-incorporated PB NPs with error bars representing the standard deviations.

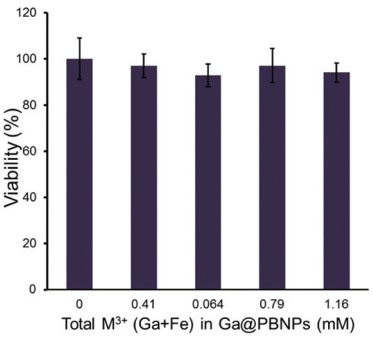

Fig. 4 Cell viability curve of Ga@PBNPs in HeLa cells after 24-hour incubation with varying amounts of NPs with error bars representing the standard deviations.

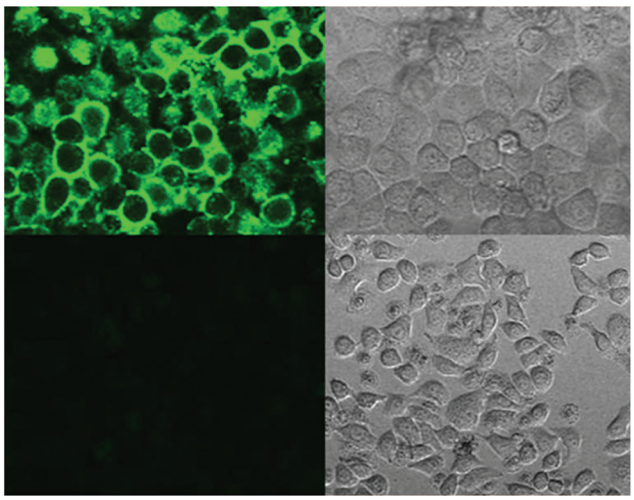

Fig. 5 Confocal microscopic images of HeLa cells: (upper left) fluorescence image of cells incubated with dye-conjugated NPs for 4 hours; (upper right) bright field image of cells incubated with dye-conjugated NPs for 4 hours; (lower left) fluorescence image of the untreated cells; (lower right) bright field image of the untreated cells.

PET or PET/MRI imaging agents. In general, small molecule-based ^{68}Ga imaging agents lack the cell-membrane permeability if no carrier or cell-targeting agent is attached to the molecules.[27] This has hampered the progress made in the past two decades in the development of ^{68}Ga-based PET radiopharmaceuticals for cellular imaging applications. The surface functionalization of a fluorescent dye on these NPs was explored to visualize cellular uptake of Ga@PBNPs in HeLa cells by confocal fluorescence microscopy. Specifically, the fluorescent dye, carboxyfluorescein (CbF), was conjugated to the surfaces of Ga@PBNPs by the EDC (*i.e.*, *N*-(3-dimethylaminopropyl)-*N*-ethylcarbodiimide hydrochloride) coupling reaction (see the Experimental section and Fig. S10 of the ESI† for details). It should be noted that free CbF dye molecules cannot penetrate the cell membrane due to their high anionic charge and poor water solubility.[39] However, HeLa cells treated with CbF-labelled Ga@PBNPs exhibited strong fluorescent signals when examined under a confocal microscope. As shown in Fig. 5, HeLa cells readily take up the CbF-conjugated Ga@PBNPs. Furthermore, the fluorescent dye molecules on the NPs act as a molecular beacon to reveal the distribution of Ga@PBNPs inside the cell. For instance, the green fluorescence signals given off by the internalized dye-labelled NPs are uniformly distributed in the cytoplasm, suggesting that endocytosis is the main mechanism for cellular uptake of these NPs. In the meantime, the fluorescent signals from the nuclei are weak, indicating a negligible nuclear uptake of the NPs in HeLa cells.

Conclusions

Incorporation of Ga-68 into the crystals of PB in the presence of two coating agents leads to the formation of $K^{68}Ga_xFe_{1-x}[Fe(CN)_6]$ NPs with remarkable thermodynamic stability as expected consistent with the parent PBNPs. The synthetic procedure described in this paper is exceptionally simple and robust, suggesting its potential for the development of this preparative method as a kit for ^{68}Ga-radiolabeling. Furthermore, the NP formulation prepared for the non-radioactive Ga-incorporated PB is highly water dispersible and hydrolytically stable at physiological pH. The cytotoxicity, cellular uptake, and proton relaxivity measurement results indicate the potential of developing such NPs as a cellular bimodal PET/MRI probe. This opens up a different avenue to address some of the challenges in the coordination chemistry of gallium.

Experimental

Reagents: All chemicals and reagents were purchased from Sigma-Aldrich and used as received without further purification unless otherwise noted.

Synthesis of the 10-GaPB NPs and bulk sample in aqueous solution

In a typical synthesis of 10% Ga(III)-doped Prussian blue nanoparticles (Ga@PBNPs), polyvinylpyrrolidone (MW-40 000; 400 mg) and citric acid (200 mg) were first added to a 40 mL aqueous solution of $Fe(NO_3)_3$ (0.9 mM) and $Ga(NO_3)_3$ (0.1 mM) while stirring. To this solution was added a 40 mL aqueous solution of $K_4[Fe(CN)_6]$ (1.0 mM) while stirring at room temperature. A clear bright blue dispersion formed immediately and the stirring was allowed to continue at room temperature for 2 hours. The pH of this dispersion was 2.2 at the end of the stirring, and was transferred into a dialysis bag and dialyzed against deionized water at room temperature for 12 hours. The product was obtained by lyophilisation. The NP sample used for preparing the TEM grids was obtained by adding an equal volume of acetone to a small aliquot of the aqueous dispersion syphoned out at the end of the stirring prior to dialysis. Centrifugation at 10 000 rpm for 10 min resulted in the formation of a small pellet, which was re-dispersed in deionized water by sonication and separated again by the addition of acetone and centrifugation. This purification process was repeated one more time to remove the soluble ions and unbound coating agents. For comparison, the bulk $KGa_{0.05}Fe_{0.95}[Fe(CN)_6]$ sample was also prepared in the absence of the coating agents. Specifically, a 40 mL aqueous solution containing both $Fe(NO_3)_3$ (1.8 mM) and $Ga(NO_3)_3$ (0.2 mM) was mixed with a 40 mL aqueous solution of $K_4Fe(CN)_6]$ (2.0 mM) with vigorous stirring at room temperature. The reaction afforded a deep blue precipitate in an hour. After stirring for another 3 hours, the precipitate was dialyzed for 24 hours in deionized water, which was replaced with fresh deionized water about every 3 hours. The purified product was then collected by lyophilisation.

Preparation of the bulk Ga@PB materials for powder X-ray studies

To determine the crystal structure, a series of bulk $KGa_xFe_{1-x}[Fe(CN)_6]$ samples (where x = 0.02–0.10) were

individually prepared by the hydrothermal reaction and included $KGa_{0.02}Fe_{0.98}[Fe(CN)_6]$, $KGa_{0.05}Fe_{0.95}[Fe(CN)_6]$, $KGa_{0.07}Fe_{0.93}[Fe(CN)_6]$ and $KGa_{0.10}Fe_{0.90}[Fe(CN)_6]$. As an example, the preparation of $KGa_{0.05}Fe_{0.95}[Fe(CN)_6]$ is as follows. A mixture of $K_4[Fe(CN)_6]\cdot 3H_2O$ (0.2747 g), $Ga(NO_3)_3$ (0.0083 g) and $Fe(NO_3)_3\cdot 9H_2O$ (0.2364 g) were added into a teflon-lined autoclave, followed by addition of 4.0 mL of distilled water and a few drops of concentrated HCl acid. The closed container was heated at 90 °C for 24 hours. The resulting blue-colored crystalline product was washed with deionized water and acetone followed by centrifugation and drying in air at room temperature for 24 hours. The other three samples were prepared similarly using the appropriate ratios of the starting materials.

TEM imaging and EDX measurements of 10-GaPB NPs

For TEM and EDX measurements, the NP sample was first suspended in deionized water by sonication. Next, a 5 μL droplet of the suspension was placed onto a carbon-coated copper TEM grid (400-mesh) and specimens were then allowed to air-dry. TEM imaging was carried out at 200 kV using a FEI Tecnai F20 field emission transmission electron microscope (TEM) equipped with an integrated scanning TEM (STEM) unit. The energy dispersive X-ray spectroscopy (EDX) results were obtained with an EDAX spectrometer in the STEM mode. The spatial resolution is <1 nm through the acquisition of high resolution high-angle dark field (HAADF) images, in which the contrast is sensitive to atomic number (Z). The elemental mapping of NPs was obtained by using the drift-corrected EDX spectra in the STEM mode for elements of interest at areas selected. These maps were generated by combining the SEM micrographs with the collected EDX spectra.

Thermogravimetric analysis of Ga@PBNPs

Thermogravimetric analysis was performed using a TA Instruments 2950 high-resolution thermogravimetric analyzer (New Castle, DE, USA) in air from room temperature to 600 °C with a heating rate of 10 °C min^{-1}. The experiments revealed the features of thermal elimination of zeolitic/coordinated water, calcination of the surface coatings of organics and decomposition of the NP core material on the basis of weight loss.

FTIR spectroscopic studies

Fourier transform infrared spectra were collected with a Bruker Vector 33 Fourier Transform Infrared Spectrophotometer using the solid samples prepared in a KBr matrix.

Powder X-ray diffraction spectroscopy (PXRD)

For routine phase identification and characterization of materials, data were collected at room temperature on a Siemens D5000 powder X-ray diffractometer using the monochromatic copper Kα radiation. Samples were ground to a fine powder and mounted on a microscopic glass slide prior to analysis. For structure determination of the bulk sample, XRD patterns were recorded using a Bruker D8 Advance X-ray powder diffractometer (Cu Kα, Ni β-filter and LynxEye PSD detector) equipped with LynxEye position detector and an incident beam Ge 111 monochromator. Powder patterns were measured from 10 to 110° 2θ with step size of 0.01446° and exposition time 800 seconds per step. Rietveld refinements were carried out using the Topas Academic software package. The atomic positions of the C and N atoms were fixed at reasonable values.

Elemental analysis studies

All atomic absorption measurements were made using a Buck Scientific 210 VGP atomic absorption spectrophotometer. The primary line of the elements was used to analyze each metal ion using hollow cathode lamps that operated at 10 mA. An air-acetylene flame was used for all measurements. When deemed necessary, the concentrations of metal ions in an aqueous solution were also measured by inductively coupled plasma atomic emission spectroscopy (ICP-OES, Perkin Elmer Optima 3300-DV ICP).

Determination of the solubility product constant for the bulk $KGa_{0.05}Fe_{0.95}[Fe(CN)_6]$

The electrical conductivity (κ) of the leachate solution of the bulk $KGa_{0.05}Fe_{0.95}[Fe(CN)_6]$ sample was measured to be 2.9 ± 1 μS cm^{-1} after the solid and solution were equilibrated for 48 hours at 20 °C. The electric conductivity of deionized water was deducted from the above value to obtain the net conductivity of the leachate solution. The equilibrium concentration of each ion was then calculated to be 2.81×10^{-10} mol dm^{-3} using the equation $\left[KGa_{0.05}Fe_{0.95}[Fe(CN)_6]_{eq} \cong \frac{\kappa}{\Lambda_m^o}\right]$. The solubility product constant of K_{sp}, defined as $[K^+] \times [M^{3+}] \times [Fe(CN)_6]$ was found to be $2.2 \pm 3 \times 10^{-29}$ mol^3 dm^{-9}, and thus showed that the leachate contained a nM level of released metal ions. These concentrations of metal ions are well below the detection limit of atomic absorption spectroscopy. Therefore, the leachate solution was pre-concentrated before the determination of metal ion concentrations were carried out by AAS. Such measurements showed that the leachate solution contained 49 ± 1 nM of iron and no gallium was detected in the pre-concentration solution.

Confocal microscopic studies of cellular uptake of Ga@PBNPs

Visualization of cellular uptake of 10-GaPB NPs was carried out with an Olympus Fluoview V1000 IX8 confocal laser-scanning microscope to confirm the internalization of nanoparticles by HeLa cells. Cells were seeded in a 6-well plate with 5×10^4 cells per well and incubated for 24 hours. Fluorescent dye-conjugated nanoparticles were then introduced to each well with the serum free fresh medium and incubated for 4 hours. The NP-incubated cells were washed three times with phosphate-buffered saline (PBS) to remove the free nanoparticles. Fresh culture medium was added to the NP-treated cells before the confocal images were acquired.

Cell viability of Ga@PBNPs

Cytotoxicity studies were performed using an MTT viability assay. HeLa cells were first seeded in a 96-well plate at a

density of 2×10^4 cells per well with the DMEM low-glucose medium and incubated for 24 hours at 37 °C in an atmosphere of 5% CO_2 and 95% air to allow the cells to attach to the surface. Cells in each well were then treated with 100 μL of fresh medium containing varying amounts of NPs and incubated for another 24 hours. Control wells contained the same medium but without the NPs. After the 24-hour incubation period, the cells were again incubated with fresh DMEM medium containing 10 μL of MTT reagent (1% w/v) for 4 more hours. The purple-colored insoluble formazan dye was formed due to the activity of mitochondrial reductase. After the MTT solution was removed, the precipitated violet crystals were dissolved in 100 μL of detergent. The absorbance was measured at 560 and 630 nm using a microplate reader. The assay results are presented as the percentage of viable cells.

T_1 and T_2 measurements

Nanoparticulate solutions of various concentrations were prepared for T_1 and T_2 measurements using a 1.5 T NMR analyzer (Mq 60 Brucker) to evaluate the proton relaxivities. For T_1 measurements, an inversion recovery gradient echo sequence with a TE = 4 ms was used. The inversion time was varied between 30–2000 ms. T_2 measurements were performed using a spin-echo sequence of TR = 10 000 ms, and TE = 10.6–340 ms.

Radioactive ^{68}Ga-labelling studies

Caution! Gallium-68 is radioactive and all work was carried out in approved laboratories following the appropriate radiation safety procedures. For the ^{68}Ga-labeling of PBNPs and radionuclide leaching studies, a solution of $K_4[Fe(CN)_6]$ (8.0 mL, 2 mM) and a solution of $Fe(NO_3)_3$ (8.0 mL, 2 mM) containing PVP (average molecular weight = 8000, 20 mg) and citric acid (20 mg) were prepared and sealed in two separate glass vials. The ^{68}Ge/^{68}Ga generator was first rinsed, and then eluted with 1 mL of 0.1 M HCl solution to obtain an activity of 1.5–1.9 mCi (55.5–70.3 MBq) of $^{68}GaCl_3$. An 100 μL aliquot of this eluent was added to a solution of $Fe(NO_3)_3$ (2 mM, 2.0 mL) containing PVP and citric acid, and then stirred for 1 minute. To a 2.00 mL solution of $Fe(NO_3)_3$ containing ^{68}Ga(III) (1.5–1.9 mCi), PVP and citric acid was added 2.0 mL of a 2 mM $K_4[Fe(CN)_6]$ solution, and this was shaken for 1 minute. A blue-colored colloidal solution containing ^{68}Ga-labelled PBNPs formed instantaneously. This solution was then transferred to a dialysis bag and sealed with clamps. The dialysis bag was immersed in a series of cups containing 100 mL of deionized water in each. Cups A, B, and C were used to rinse off any unbound radioisotopes, and then cup D was used to examine the stability of the ^{68}Ga-labelled PBNPs. After the first three cups were taken, the fourth cup, D (100.0 mL deionized water), was used to examine the stability of the compound. Aliquots of 5.00 mL were removed from leachates A, B, and C, and counted on a high purity germanium (HPGe) detector. For cup D, 0.5 mL aliquots were removed at selected time intervals (*i.e.*, 5, 10, 15, 20, 30, 45, and 60 minutes) and counted using a HPGe detector. The radioactivity counting was carried out by gamma spectroscopy using the 511 keV annihilation photons associated with ^{68}Ga. The activity of the leachate solutions was converted to a percentage of the original activity incorporated into the PBNPs. Triplicate studies were performed. All of the dialysis samples were below the limit of detection for the HPGe. The original samples on average contained 3.07×10^6 cpm. This high number of counts indicates that >99.9% of the activity was bound and remained inside the dialysis bag.

Acknowledgements

We thank NIH-NCI for financial support (1R21CA143408-01A1); trainee support was provided from the National Science Foundation under IGERT award DGE-0965983 (M. D. Gott). The Ga-68 was made available from the University of Missouri Research Reactor (MURR) with the radiochemistry studies performed at MURR. The TEM data were obtained using the Cryo TEM Facility at Liquid Crystal Institute, KSU supported by the Ohio Research Scholars Program.

Notes and references

1 M. N. Wernick and J. N. Aarsvold, *Emission Tomography: The fundamental of PET and SPECT*, Elsevier Academic Press, 2004.
2 D. Brasse and A. Nonat, *Dalton Trans.*, 2015, **44**, 4845–4858.
3 R. Alberto, *Comp. Coord. Chem. II*, 2004, **5**, 127.
4 S. S. Jurisson and J. D. Lydon, *Chem. Rev.*, 1999, **99**, 2205–2218.
5 S. Liu and D. S. Edwards, *Chem. Rev.*, 1999, **99**, 2235.
6 K. Schwochau, *Angew. Chem., Int. Ed. Engl.*, 1994, **33**, 2258.
7 M. D. Bartholomä, A. S. Louie, A. S. J.-F. Valliant and J. Zubieta, *Chem. Rev.*, 2010, **110**, 2903–2920.
8 I. Velikyan, *Theranostics*, 2014, **4**, 47–80.
9 S. Bhattacharyya and M. Dixit, *Dalton Trans.*, 2011, **40**, 6112–6128.
10 M. Fani, J.-P. André and H. R. Maecke, *Contrast Media Mol. Imaging*, 2008, **3**, 53–63.
11 B. P. Burke, G. S. Clemente and S. J. Archibald, *J. Labelled Compd. Radiopharm.*, 2014, **57**, 239–243.
12 M. Pagou, I. Zerizer and A. Al-Nahhas, *Hell J. Nucl. Med.*, 2009, **12**, 102–105.
13 M. D. Bartholomä, *Inorg. Chim. Acta*, 2012, **389**, 36–51.
14 W. R. Harris and A. E. Martell, *Inorg. Chem.*, 1976, **15**, 713–720.
15 S. M. Moerlein and M. J. Welch, *Int. J. Nucl. Med. Biol.*, 1981, 277–287.
16 G. E. Jackson and M. J. Byrne, *J. Nucl. Med.*, 1996, **37**, 379–386.
17 S. Wang, R. J. Lee, C. J. Mathias, M. A. Green and P. S. Low, *Bioconjugate Chem.*, 1996, **7**, 56–62.
18 L. G. Luyt and J. A. Katzenellenbogen, *Bioconjugate Chem.*, 2002, **13**, 1140–1145.

19 J. Šimeček, O. Zemek, P. Hermann, J. Notni and H.-J. Wester, *Mol. Pharmaceutics*, 2014, **11**, 3893–3903.
20 K. Ogawa, J. Yu, A. Ishizaki, M. Yokokawa, M. Kitamura, Y. Kitamura, K. Shiba and A. Odani, *Bioconjugate Chem.*, 2015, **26**, 1561–1570.
21 R. Weissleder and V. Ntziachristos, *Nat. Med.*, 2003, **9**, 123–128.
22 X. Gao, Y. Cui, R. M. Levenson, L. W. K. Chung and S. Nie, *Nat. Biotechnol.*, 2004, **22**, 969–976.
23 A. P. Alivisatos, W. Gu and C. Larabell, *Annu. Rev. Biomed. Eng.*, 2005, **7**, 1–22.
24 N. L. Rosi and C. A. Mirkin, *Chem. Rev.*, 2005, **105**, 1547–1562.
25 S. K. Nune, P. Gunda, P. K. Thallapally, Y.-Y. Lin, M. L. Forrest and C. J. Berkland, *Expert Opin. Drug Delivery*, 2009, **6**, 1175–1194.
26 B. P. Burke, N. Baghdadi, G. S. Clemente, N. Camus, A. Guillou, A. E. Kownacka, J. Domarkas, Z. Halime, R. Tripier and S. J. Archibald, *Faraday Discuss.*, 2014, **175**, 59–71.
27 B. P. Burke, N. Baghdadi, A. E. Kownacka, S. Nigam, M. M. Al-Yassiry, J. Domarkas, M. Lorch, M. Pickles, P. Gibbs, R. Tripier, C. Cawthorne and S. J. Archibald, *Nanoscale*, 2015, **7**, 14889–14896.
28 M. Shokouhimehr, E. S. Soehnlen, A. Khitrin, S. Basu and S. D. Huang, *Inorg. Chem. Commun.*, 2010, **13**, 58–61.
29 M. Shokouhimehr, E. S. Soehnlen, J. Hao, M. Griswold, C. Flask, X. Fan, J. P. S. Basilion, S. Basu and S. D. Huang, *J. Mater. Chem.*, 2010, **20**, 5251–5259.
30 M. S. Kandanapitiye, B. Valley, L. D. Yang, A. M. Fry, P. M. Woodward and S. D. Huang, *Inorg. Chem.*, 2013, **52**, 2790–2792.
31 H. J. Buser, D. Schwarzenbach, W. Petter and A. Ludi, *Inorg. Chem.*, 1977, **16**, 2704–2710.
32 K. R. Dunbar and R. A. Heintz, *Prog. Inorg. Chem.*, 1996, **45**, 283–391.
33 *TOPAS Academic, General Profile and Structure Analysis Software for Powder Diffraction Data*, Bruker AXS, Karlsruhe, Germany, 2004.
34 A. Widmann, H. Kahlert, I. Petrovic-Prelevic, H. Wulff, J. V. Yakhmi, N. Bagkar and F. Scholz, *Inorg. Chem.*, 2002, **41**, 5706–5715.
35 H. L. Clever and F. J. Johnston, *J. Phys. Chem. Ref. Data*, 1980, **9**, 753–766.
36 V. S. Perera, L. D. Yang, J. Hao, G. Chen, B. O. Erokwu, C. A. Flask, P. Y. Zavalij, J. P. Basilion and S. D. Huang, *Langmuir*, 2014, **30**, 12018–12026.
37 P. Caravan, *Chem. Soc. Rev.*, 2006, **35**, 512–523.
38 V. S. Perera, G. Chen, Q. Cai and S. D. Huang, *Analyst*, 2016, **141**, 2016–2022.
39 T. O. Pangburn, K. Georgiou, F. S. Bates and E. Kokkoli, *Langmuir*, 2012, **28**, 12816–12830.